RSC Advances

PAPER

View Article Online
View Journal | View Issue

Cite this: *RSC Adv.*, 2021, **11**, 71

Application of electroactive Au/aniline tetramer–graphene oxide composites as a highly efficient reusable catalyst

Guan-Hui Lai,[a] Yi-Chen Chou,[b] Bi-Sheng Huang,[a] Ta-I. Yang[c] and Mei-Hui Tsai *[ad]

Received 7th October 2020
Accepted 13th November 2020

DOI: 10.1039/d0ra08535a

rsc.li/rsc-advances

This study proposes a cost-effective, energy-saving, and green process that uses π–π interactions to modify graphene oxide (GO), and the conjugate structure of aniline tetramer (AT) to enhance the dispersion of GO. Au/aniline tetramer–graphene oxide (Au/ATGO) composites were synthesized and applied as a catalyst in this study. The adsorption of AT on GO, *via* π–π interaction, formed ATGO composites. Subsequently, the amine group on ATGO was stably anchored on Au nanoparticles (Au NPs) to form Au/ATGO composites. The Au/ATGO composites were characterized and the electroactive properties determined by Fourier-transform infrared spectroscopy, X-ray photoelectron spectroscopy, transmission electron microscopy, and cyclic voltammetry. The Au/ATGO composites showed excellent performance and stability as catalysts when applied for the reduction of nitrophenol to aminophenol within 225 s and the rate constant was 0.02 s^{-1}. The activation energy for the reduction of 4-NP and 2-NP was 48.10 and 68.71 kJ mol^{-1}, respectively. Following a recycling test repeated 20 times, the Au/ATGO composites maintained a conversion rate higher than 94%.

Introduction

Conducting polymers such as polyaniline (PANI), polypyrrole, and polythiophene are interesting materials that have been studied and applied in various areas of technology. Owing to its facile synthesis process, unique redox properties, excellent environmental stability, good electrical conductivity, and simple acid–base doping/dedoping chemistry,[1–3] PANI is one of the most promising types of polymer types used for the production of anticorrosion coatings,[4] chemical sensors,[5] catalysis,[6] and supercapacitors.[7] However, the application of PANI has some drawbacks such as low solubility in the most common solvents, infusibility, and difficulty in processing.[8] Also, its electrical conductivity decreases over a long cycle time.[9] To solve these problems, an aniline oligomer can be used in place of PANI because it not only retains the advantageous properties of PANI, but it also exhibits much better processability.[10,11] Kaner *et al.* mentioned that aniline tetramer (AT) is the shortest oligomer with a structure similar to that of PANI.[12] It is easy to control the morphology and size *via* the doping. Various crystalline nanostructures such as fibers, sheets, porous structure, and hollow spheres can be obtained by controlling the nucleation of the crystals and the non-covalent interactions between the doped oligomers.[13] Yan *et al.* synthesized aniline oligomer/graphene oxide (GO) to enhance the electrochemical cycling stability of a supercapacitor from 84.2% to above 95.1%, after 2000 cycles. They mentioned that AT is a polymer with a short-chain, and the bonding itself may be weak. GO is a material with a 2D micrometer-sized structure, and it can support AT to prevent dissolution.[9] Li *et al.* used the tetraphenylethylene group to fabricate soluble reduced graphene oxide (rGO) composites through efficient π–π stacking interactions; stable dispersions of graphene sheets in organic solvents could also be prepared. These findings provide new opportunities for the development of graphene-based materials that may have applications in optoelectronic devices, chemical sensors, and biomedical areas.[14] Han *et al.* combined various aniline oligomers (dimer, trimer, and tetramer) with graphene to enhance the electrical and electrochemical performance of asymmetric supercapacitors. They observed that the AT exhibited higher areal capacitance, volumetric capacitance, and energy density than the samples fabricated from the dimer and trimer electrodes. Significant improvements in the performance of the tetramer sample were highly related to the improved electrical conductivity and structural stability when compared with the samples containing the trimer and dimer electrodes.[15]

[a]*Ph. D. Program, Graduate Institute of Precision Manufacturing, National Chin-Yi University of Technology, Taichung, 41170, Taiwan. E-mail: tsaimh@ncut.edu.tw*

[b]*Department of Applied Cosmetology, Hungkuang University, Taichung 44302, Taiwan. E-mail: jacs1@hk.edu.tw*

[c]*Department of Chemical Engineering, Chung Yuan Christian University, Chung Li 32023, Taiwan. E-mail: taiyang@cycu.edu.tw*

[d]*Department of Chemical and Materials Engineering, National Chin-Yi University of Technology, Taichung, 41170, Taiwan*

Recently, chemical amino functional groups have been used as agents to anchor nanoparticles on substrates such as carbon nanotube (CNT),[16] graphene,[17,18] SiO_2,[19] and zirconium phosphate (ZrP)[20] have been studied. Ou *et al.* used 1-pyrenemethylamine as the inter-linker to synthesize CNT–Au composites. The alkylamine substituent of 1-pyrenemethylamine binds to an Au nanoparticle (Au NP), while the pyrene chromophore was non-covalently attached to the sidewall of a carbon nanotube *via* π–π interaction. Using this strategy, Au NPs within the size range of 2–4 nm can be closely assembled on multiwalled carbon nanotubes.[21] Yao *et al.* modified the surface GO using N^1-(3-trimethoxysilylpropyl)diethylene triamine. The amine groups of the functionalized GO could effectively template the Au NPs assembly on the graphene surface with a high density and good dispersity. The TEM images of the modified GO show that the Au NPs maintained their original size, and they were well-anchored on the graphene surfaces with an average size of 15 nm.[22] Furthermore, Yao *et al.* also used a variety of amine end group silane coupling agents that modified GO lead to GO/Au composites by controlling the grafting density of Au NPs. These different functional groups enabled the alteration of the grafting density of Au NPs which tailored the Au NPs for different catalytic applications. All GO/Au composites showed high efficiency in catalyzing a hydrogenation reaction, completing the reaction within 16 min. After 7 catalytic cycles of testing, no signs of detachment or aggregation were observed.[23] These methods demonstrated the efficient inhabitation of Au NPs aggregation and the improvement of its catalytic activities.

In previous literature, graphene or GO were modified using silane agents, polymers, and so on following several complicated steps that require high cost, energy consumption, and the process is time-consuming. Herein, we used π–π interactions to modify GO. This method is cost-effective, saves energy, and requires the use of environmentally friendly solvents. To the best of our knowledge, the use of aniline tetramer–graphene oxide (ATGO) composites containing Au NPs as a catalyst have seldomly been studied. In this study, the conjugate structure of AT enhanced the dispersion of GO in the solvent through π–π interactions. Subsequently, a multi-amino functional group on ATGO was used to stably anchor Au NPs to form Au/ATGO composites. The Au/ATGO composites were characterized by field-emission transmission electron microscopy (TEM), Fourier-transform infrared (FTIR) spectroscopy, UV-visible (UV-Vis) spectroscopy, X-ray photoelectron (XPS) spectroscopy, and cyclic voltammetry (CV). The Au/ATGO composites showed good stability against agglomeration and excellent catalytic activity in a model reduction reaction of 4-NP into 4-AP, and 2-nitrophenol (2-NP) to 2-aminophenol (2-AP). The catalytic activity of the Au/ATGO composites was over 94% after 20 cycles.

Experimental

Materials

Graphite and *N*-phenyl-*p*-phenylenediamine were purchased from Alfa Aesar. Iron(III) chloride, hydrochloric acid (HCl), sulfuric acid (H_2SO_4), hydrogen peroxide (H_2O_2), and alcohol were obtained from ECHO chemical company. Potassium permanganate ($KMnO_4$) was obtained from TCI. Tetrachloroauric(III) acid trihydrate ($HAuCl_4$), sodium citrate, sodium borohydride ($NaBH_4$), 4-nitrophenol, and 2-aminophenol were procured for Sigma-Aldrich.

Synthesis of ATGO composites

GO was prepared from graphite by the modified Hummers method.[24,25] 3 g of graphite was mixed with 360 mL H_2SO_4 and 40 mL H_3PO_4 in a flask, and the temperature was raised to 50 °C followed by the addition of 18 g of $KMnO_4$. The mixture was continuously stirred overnight, and then 10 mL of H_2O_2 was added into the mixture. The fully oxidized suspension was poured into a large amount of deionized (DI) water, it was then centrifuged and washed to obtain the GO powder. AT was synthesized using a method we had previously developed.[26] *N*-Phenyl-*p*-phenylenediamine (0.01 mol) was dissolved in 200 mL of 1 M HCl. Subsequently, a solution containing iron(III) chloride (0.01 mol) was added to the HCl containing *N*-phenyl-*p*-phenylenediamine while it was stirred in an ice bath. The resulting solution was allowed to react for another 4 h. The precipitate was filtered and washed with distilled water several times. The obtained AT was freeze-dried overnight. ATGO was prepared by simultaneous dispersion of 10 mg AT and 100 mg GO in 250 mL of alcohol and stirred for 24 h. The ATGO was washed three times with alcohol by centrifugation and resuspension, it was then dried at 70 °C in an oven for 24 h, and subsequently ground into a fine powder with a mortar and pestle.

Fabrication of Au/ATGO composites

100 mL of $HAuCl_4$ (1 mM) aqueous solution was refluxed and stirred. 10 mL of sodium citrate (38.8 mM) aqueous solution was rapidly added to the boiling solution, and this resulted in a color change from yellow to wine red. The resulting solution was stirred for 10 min, then the heat source was removed. The solution was continuously stirred until the solution cold down to room temperature to obtain the Au NPs solution.[20] To prepare the Au/ATGO composites, Au NPs solution (50 mL) was mixed with ATGO (10 mg) at room temperature and stirred overnight. The final Au/ATGO composites were collected by centrifugation and washed with DI water. The schematic representation of the synthesis process is shown in Scheme 1.

Characterization

The FTIR spectra were recorded with a FTIR-4600 spectrometer (Jasco, Japan), the resolution used in the measurements and the number of scans were 4 cm^{-1} and 64 scans, respectively. The mass spectra were obtained on a triple quadrupole mass spectrometer with an ESI source (Thermo Scientific, United States). The

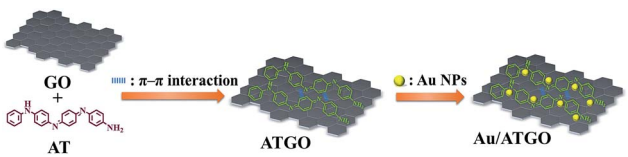

Scheme 1 Synthesis of Au/ATGO composites.

UV-Vis absorption spectra were measured using a V-750 spectrometer (Jasco, Japan). The XPS analysis was performed using a PHI 5000 VersaProbe (ULVAC-PHI, Japan). The morphology and crystal structures of the samples were observed by TEM operated at 200 kV. Energy dispersive X-ray (EDX) mapping analysis was carried out on the TEM measurement (JEOL JEM-2100F, Japan). Thermogravimetric analysis (TGA) was conducted in air and nitrogen atmosphere at a heating rate of 20 °C min^{-1} over a temperature range of 30–800 °C using a TA Q500 (TA Instrument, United States). Electrochemical experiments were performed using a CHI 6273E electrochemical analyzer with a conventional three-electrode system (CH Instruments, United States).

Catalytic activity

To study the catalytic performance of the Au/ATGO composites, the composite was applied in the reduction reaction of 4-NP and 2-NP. $NaBH_4$ was used as a hydrogen generation source in water. 1 mg of Au/ATGO composites was dispersed in 3 mL of 4-NP or 2-NP solution (0.1 mM). Then a freshly prepared 0.15 mL solution of $NaBH_4$ (100 mM) was added. The molar ratio of 4-NP (2-NP)/$NaBH_4$ is 0.02. The mixture was immediately into a quartz cuvette and the UV-Vis absorption spectra were recorded to monitor changes in the reaction mixture.

Results and discussion

Characterization of AT, GO, ATGO, and Au/ATGO composites

The mass spectra of AT are shown in Fig. 1(a). The characterizations of AT were conducted as follows: ion trap-MS *m*/*z*: $[M + H]^+$ calculated for $C_{24}H_{20}N_4$ = 364.3. Found 365.3. The FTIR spectra of GO, AT, and ATGO are shown in Fig. 1(b). From the FTIR spectrum of GO, the peak at 1041 cm^{-1} was ascribed to C–O–C bonding, and the peaks at 3373, 1725, and 1620 cm^{-1} signified the presence of –OH, C=O, and C=C functional groups, respectively, which indicates that abundant oxygen-containing groups existed on the surface of GO.[24,27] The peak between 3314 and 3209 cm^{-1} can be attributed to the N–H stretching vibration, while those at 3032 cm^{-1} can be attributed to the C–H stretching vibration.[28] The AT showed N=Q=N (quinoid ring) and N=B=N (benzenoid ring) bands at 1594 and 1504 cm^{-1}, respectively.[29,30] The peak at 1309 cm^{-1} can be attributed to C–N stretching vibration.[31,32] The other peaks at 1165, 834, and 748 cm^{-1} are due to C–H bending vibrations.[33] The FTIR spectrum of the ATGO contains the characteristic peaks of AT and GO.

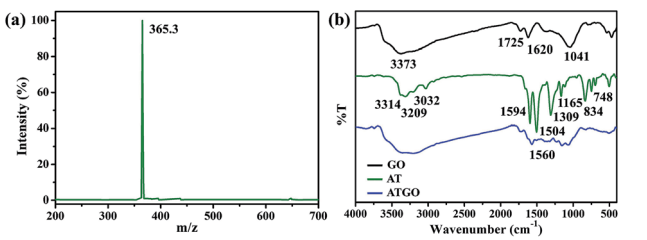

Fig. 1 (a) Mass spectra of AT. (b) FTIR spectra of GO, AT, and ATGO.

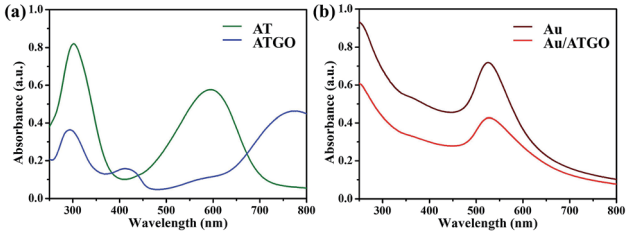

Fig. 2 UV-Vis spectra of (a) AT and ATGO, and (b) Au and Au/ATGO composites.

The UV-Vis spectra of AT and ATGO supernatants are shown in Fig. 2(a). The two absorption peaks at 312 and 598 nm in the UV-Vis spectrum of AT are attributed to the π–π* transition of the benzene unit and the π_B–π_Q transition of benzenoid to quinoid, respectively.[34,35] For ATGO, an absorption peak at 304 nm similar to that in the UV-Vis spectrum of AT was observed. A new absorption peak at 415 nm was observed, and the peak was attributed to the polaron → π* band transitions, and the peak at 785 nm was ascribed to the π → polaron transitions, which demonstrated that GO was doped on the AT.[36,37] Pristine Au NPs with a particle size of 15 nm show a surface plasmon resonance peak at approximately 525 nm in the visible spectrum.[38] The surface plasmon resonance peaks of the assembled Au/ATGO composites become much broader owing to the strong inter-particle coupling of closely packed particles (Fig. 2(b)).

XPS was also used to detect the compositions of the samples. The XPS profiles of GO, ATGO, and Au/ATGO composites are shown in Fig. 3. The characteristic peaks of C 1s and O 1s were observed in the profile of the three samples at 286.0 and 533.0 eV, respectively.[39] A different peak assigned to N 1s was observed in the XPS profile of ATGO. The N 1s peak at 398.0 eV indicates the presence of AT.[40,41] The existence of Au was confirmed by the Au 4f peak at approximate 87.0 eV, which is enlarged in Fig. 3(b). The diffused peaks with binding energies of 84.0 and 87.8 eV correspond well with Au $4f_{7/2}$ and Au $4f_{5/2}$ in the metallic state, respectively.[42]

The morphologies of the GO, Au, Au/ATGO composites were characterized by TEM. As shown in Fig. 4(a), a typical 2D GO nanosheet by itself contains wrinkled structures, and the TEM image of pure Au NPs with a diameter of 15 nm is shown in Fig. 4(b). After the growth of Au NPs on the surface of the ATGO, the morphology of the ATGO remained unaltered. The TEM images of the Au/ATGO composites (Fig. 4(c and d)) clearly indicate that

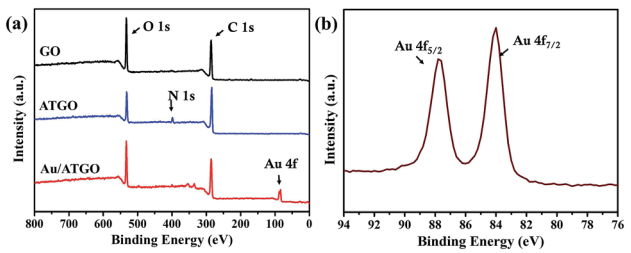

Fig. 3 XPS profiles of (a) GO, ATGO, and Au/ATGO; Au 4f spectra of (b) Au/ATGO composites.

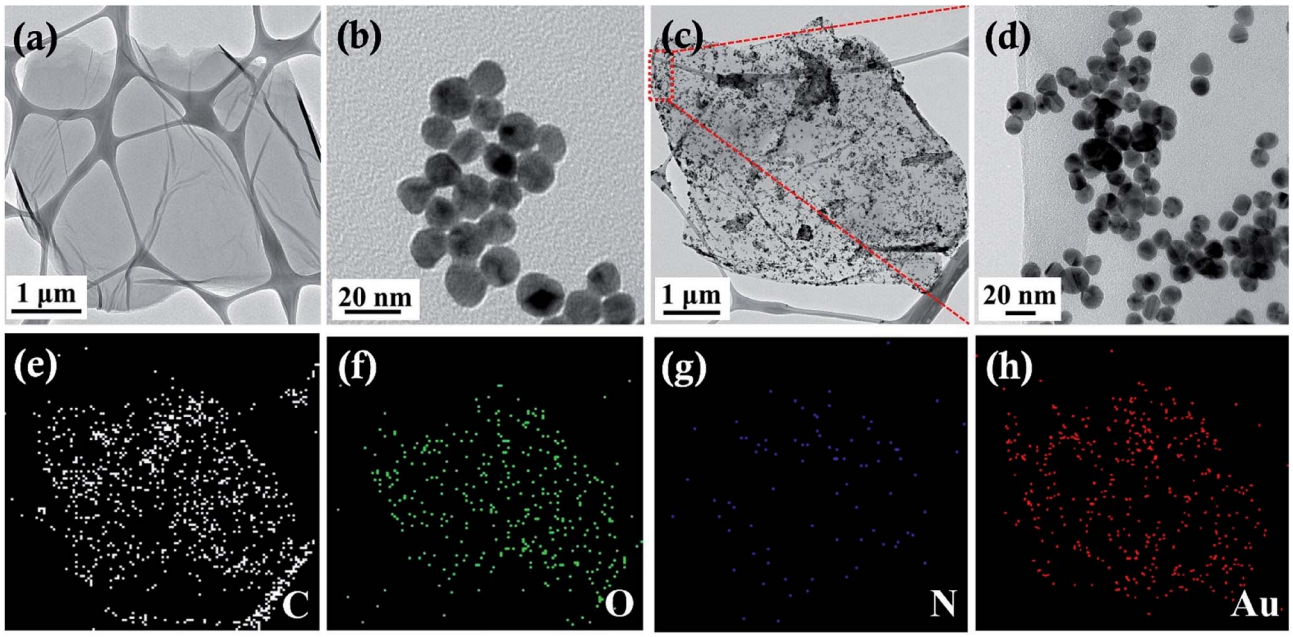

Fig. 4 TEM images of (a) GO, (b) Au, (c) Au/ATGO composites, (d) high magnification of Au/ATGO composites shown in the area in (c), and (e–h) elemental mapping images.

spherical Au NPs were anchored and well-distributed on the surface of the ATGO. The elemental mappings of the Au/ATGO composites shown in Fig. 4(e–h) indicates that the nanoparticles were caused by the Au NPs anchored on the ATGO.

The thermogravimetry analysis curves of GO, ATGO, and Au/ATGO composites showed an notable weight loss between 150 and 250 °C, which is attributed to the pyrolysis of the labile oxygen-containing functional groups that yielded CO, CO_2, and steam.[43] The TGA curves of GO and ATGO show a complete decomposition of carbon at approximately 525 °C. In contrast, carbon was completely decomposed in the Au/ATGO composites at a lower temperature of approximately 448 °C. A residual mass of approximately 33.4% indicates the loading of Au NPs in the Au/ATGO composites (Fig. 5).[44]

Electrical properties of ATGO and Au/ATGO composite

To study the redox behavior of ATGO and Au/ATGO composites, two samples were systematically examined by CV in 40 mL of 1.0 M H_2SO_4 and a potential ranging from −0.2 to 1.0 V at a scan rate of 50 mV s^{-1}. Fig. 6(a) shows the CV curves of the ATGO and Au/ATGO composites. Both the ATGO and Au/ATGO composites show two distinct pairs of redox peaks. This observation could be attributed to the change in the molecular structure of AT. The first oxidation peak corresponded to the transition from the leucoemeraldine base to the emeraldine base (EB), the second peak corresponded to the transition from EB to the pernigraniline base, as shown in Fig. 6(b).[45,46] Furthermore, with the Au NPs acting as electrically conductive bridges inside the Au/ATGO composites, the diffusion length of the electrolyte ions was significantly reduced, resulting in an enhanced current when compared with that of the ATGO.[47]

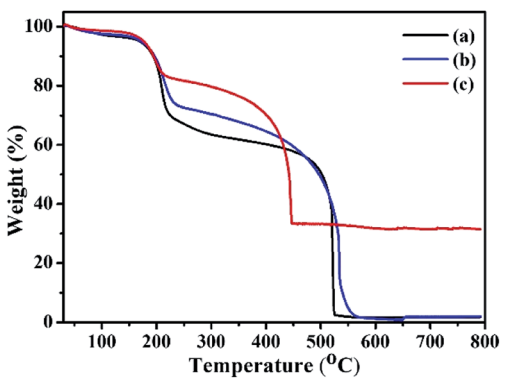

Fig. 5 TGA curves of (a) GO, (b) ATGO, and (c) Au/ATGO composites.

Catalytic characterization of Au/ATGO composites

Currently, water pollution and scarcity of consumable water resources have led to damaging consequences around the world, and this posed a threat to human life. Among the harmful toxins and compounds in polluted water, nitrophenol is one of the 126 priority pollutants listed by the United States

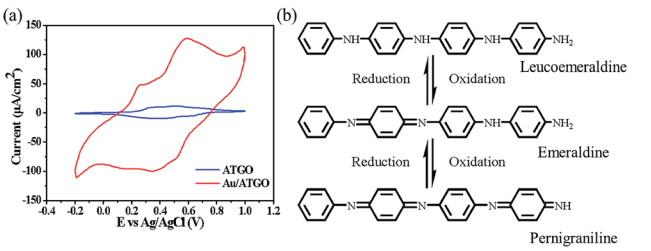

Fig. 6 Representative CV curves of the (a) ATGO and Au/ATGO composites in H_2SO_4 solution. Scan rate: 50 mV s^{-1}. (b) Molecular structures of ATGO at various oxidation states.

Environmental Protection Agency.[48,49] It is commonly found in wastewaters of industries that manufacture pesticide, dye, pharmaceutical, and petrochemical products.[50] Aminophenol is an important intermediate in the preparation of several analgesics and antipyretic drugs.[51,52] It is a strong reducing agent, and it is used as a corrosion inhibitor in paints as well as photographic development.[53,54] Due to the aforementioned reasons, it is important to convert nitrophenol to aminophenol. Compared to other conversion routes, the method where $NaBH_4$ is used as a reducing agent in an aqueous medium under mild conditions is relatively simple and quick.[55]

To evaluate the catalytic activity of the synthesized nanocatalyst samples, reduction of 4-NP and 2-NP by $NaBH_4$ was first selected as the model reaction, which can be monitored by time-dependent UV-Vis spectroscopy. The aqueous solution of 4-NP is light yellow and it shows a strong absorption peak at 316 nm. After the addition of $NaBH_4$, a color change from light yellow to deep yellow was observed, and a strong absorption peak at 400 nm appeared owing to the formation of 4-nitrophenolate ions (Fig. 7(a)).[56,57] Furthermore, in the blank test, no change in the absorption intensity was observed for a long period with $NaBH_4$, which indicates that the reduction reaction did not occur without the addition of the catalyst. After the addition of the Au/ATGO composites, the absorption peak at 400 nm owing to 4-nitrophenolate ions gradually decreased; at the same time, a new peak was observed at 296 nm indicating the formation of 4-AP.[58] The Au/ATGO composites showed high activity and completed the reaction in 225 s (Fig. 7(b)).

For a comparative study, the apparent rate constants were calculated for all the catalyst samples. Since $NaBH_4$ (100 mM) was used in excess and remained approximately constant throughout the progression of the reaction, pseudo-first-order kinetics was applied for evaluating the apparent rate constants (k_{app}). The k_{app} values were calculated from linear plots of $\ln(C_t/C_0)$ *vs.* reduction time t (Fig. 7(c)). Here, C_t and C_0 represent the absorbance of 4-NP after time $t = t$ and $t = 0$, which can be considered equivalent to the concentration at time $t = t$ (C_t) and $t = 0$ (C_0), respectively.[59,60] The linear relationship between $\ln(C_t/C_0)$ and t indicates the pseudo-first-order reduction of 4-NP by the Au/ATGO composites, and the calculated value of k_{app} was 0.021 s^{-1}. A comparative study of 4-NP reduction with other catalysts is given in Table 1. Compare to other catalyst materials containing Au nanoparticles, Au/ATGO showed high catalytic performance. In this study, we also carried out a series of reactions for the reduction of 4-NP in the presence of Au/ATGO composites to obtain thermodynamic parameters that reveal how the reaction temperature can affect the kinetics of such a reaction. Apparently, the reaction rate is quite sensitive to temperature and the value of the rate constant, k, increases with temperature. In addition, according to the Arrhenius equation: $\ln k = \ln A - E_a/RT$, the activation energy (E_a) can be obtained from the slope based on the linear fitting of $\ln k$ *versus* $1/T$.[61] The activation energy of the reaction catalyzed by Au/ATGO composites was determined from the Arrhenius plot to be 48.10 kJ mol^{-1}.

Table 1 Comparative characteristics and catalytic performance of catalyzers in the reported literature

Catalyzer	mg	Degradation time (s)	Rate constant (min^{-1})	Ref.
Au/GO	0.02	720	0.15	23
Au/ZrP–SH	7	420	0.19	64
Au/EPA	0.5	270	0.42	65
Au/carbon black	10	300	0.83	42
Au/ZrP–NH_2	1	180	1.08	20
Ni–Au/HNO_3–CB[a]	5	180	1.96	56
Au/ATGO	1	225	1.26	This work

[a] CB: carbon black.

Based on the above results, we also used the Au/ATGO composites to perform the catalytic reduction of 2-NP, as shown in Fig. 8. The yellow solution of 2-NP exhibited two distinct absorption peaks at 278 and 350 nm. Following the addition of $NaBH_4$, a color change from light yellow to deep yellow was observed, and the absorption peaks shifted to 282

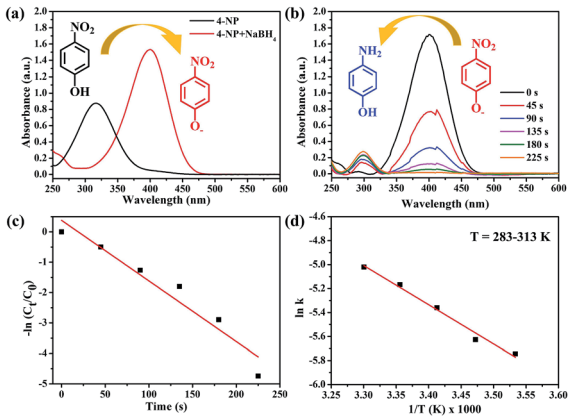

Fig. 7 UV-Vis spectra of (a) 4-NP before and after addition of $NaBH_4$, (b) time-dependent reduction process after the addition of Au/ATGO composites in the reaction. 4-NP reduction catalyzed by Au/ATGO composites in the presence of $NaBH_4$. (c) The plot of $-\ln(C_t/C_0)$ *versus* time, and (d) the plot of $\ln k$ *versus* $1/T$ based at different temperatures.

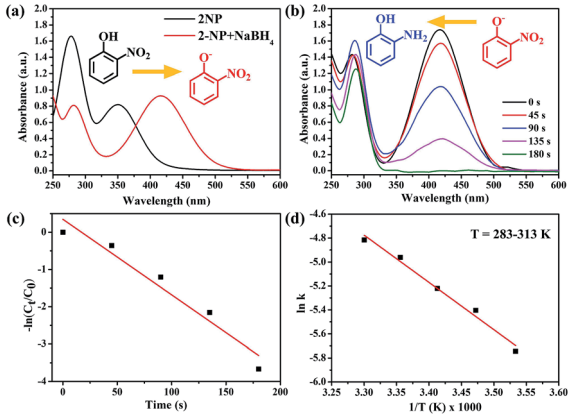

Fig. 8 UV-Vis spectra of (a) 2-NP before and after addition of $NaBH_4$, (b) time-dependent reduction process after the addition of Au/ATGO composites in the reaction. 2-NP reduction catalyzed by Au/ATGO composites in the presence of $NaBH_4$ (c) the plot of $-\ln(C_t/C_0)$ *versus* time, and (d) the plot of $\ln k$ *versus* $1/T$ based on different temperature.

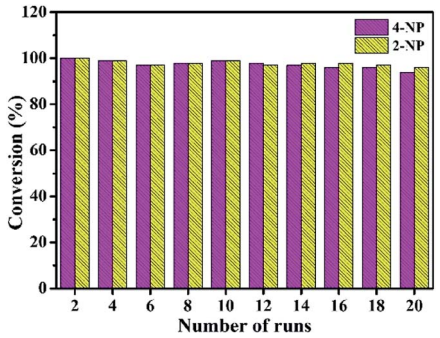

Fig. 9 Recycling stability of the Au/ATGO composites system for catalytic reduction of nitrophenol to aminophenol.

and 416 nm owing to the formation of 2-nitrophenolate ions (Fig. 8(a)).[62] However, adding Au/ATGO composites to a 2-NP and $NaBH_4$ mixed solution caused a reduction in the intensity of the peak at 416 nm over time, indicating the formation of 2-AP.[63] As shown in Fig. 8(b), it took 180 s for the complete reduction of 2-NP. As shown in Fig. 8(c), the k_{app} value was 0.02 s^{-1} and the E_a was 68.71 kJ mol^{-1}. The results indicate that Au/ATGO composites exhibited significant activity during the reduction of nitrophenols with $NaBH_4$ as the hydrogen donor.

Recycling tests

As shown in Fig. 9, the Au/ATGO composites can be easily separated by sedimentation and reused under the same reaction conditions. The reduction rate of 4-NP to 4-AP, and 2-NP to 2-AP was maintained above 94% and 96%, respectively, after 20 cycles; this indicates the high stability and reusability of the resulting Au/ATGO composites system.

Conclusions

In this study, stable, and reusable Au/ATGO composites were prepared and used as catalysts for the degradation reaction of nitrophenol. The synthesis of ATGO was based on the π–π interaction of GO and AT. Subsequently, the amine group on ATGO stably anchored Au nanoparticles (Au NPs) to form Au/ATGO composites. Furthermore, because of the growth of the Au NPs based on Au seeds, the catalyst was reused for more than 20 cycles and stored for over 2 months, while maintaining approximately the same catalytic performance (conversion rate above 94%). The Au/ATGO composites showed many advantages including high catalytic activity and excellent recyclability that makes them attractive for several other applications.

Conflicts of interest

There are no conflicts to declare.

Acknowledgements

We would like to thank the Ministry of Science and Technology, Taiwan under grant numbers MOST 108-2917-I-167-001, MOST 108-2221-E-167-020, MOST 108-2731-M-005-001, and MOST 109-2637-E-241-004 for their financial support. This material is based on work supported by the Research Center for Circular Economy at Chung-Yuan Christian University, Taiwan. We thank the Instrument Center of National Chung Hsing University for the help with the SEM, TEM, and XPS measurements.

References

1 T. Hou, P. Gai, M. Song, S. Zhang and F. Li, *J. Mater. Chem. B*, 2016, **4**, 2314–2321.
2 T. S. Radoman, J. V. Džunuzović, B. N. Grgur, M. M. Gvozdenović, B. Z. Jugović, D. S. Miličević and E. S. Džunuzović, *Prog. Org. Coat.*, 2016, **99**, 346–355.
3 T. C. Huang, J. M. Yeh and C. Y. Lai, in *Advances in Polymer Nanocomposites*, ed. F. Gao, Woodhead Publishing, 2012, pp. 605–638.
4 C.-H. Chang, T.-C. Huang, C.-W. Peng, T.-C. Yeh, H.-I. Lu, W.-I. Hung, C.-J. Weng, T.-I. Yang and J.-M. Yeh, *Carbon*, 2012, **50**, 5044–5051.
5 I. Fratoddi, I. Venditti, C. Cametti and M. V. Russo, *Sens. Actuators, B*, 2015, **220**, 534–548.
6 L. Sun, S. Peng, L. Jiang, Y. Zheng, X. Sun, H. Su and C. Qi, *Colloid Polym. Sci.*, 2019, **297**, 651–659.
7 C.-M. Chang, C.-J. Weng, C.-M. Chien, T.-L. Chuang, T.-Y. Lee, J.-M. Yeh and Y. Wei, *J. Mater. Chem. A*, 2013, **1**, 14719–14728.
8 M. Chi, S. Wang, Y. Liang, D. Chao and C. Wang, *J. Colloid Interface Sci.*, 2014, **423**, 7–12.
9 J. Yan, L. Yang, M. Cui, X. Wang, K. J. Chee, V. C. Nguyen, V. Kumar, A. Sumboja, M. Wang and P. S. Lee, *Adv. Energy Mater.*, 2014, **4**, 1400781.
10 Y. Zhou, E. B. Berda, Q. Ma, X. Liu, C. Wang and D. Chao, *ChemElectroChem*, 2019, **6**, 5293–5300.
11 T.-C. Huang, T.-C. Yeh, H.-Y. Huang, W.-F. Ji, Y.-C. Chou, W.-I. Hung, J.-M. Yeh and M.-H. Tsai, *Electrochim. Acta*, 2011, **56**, 10151–10158.
12 Y. Wang, H. D. Tran, L. Liao, X. Duan and R. B. Kaner, *J. Am. Chem. Soc.*, 2010, **132**, 10365–10373.
13 Y. Wang, J. Liu, H. D. Tran, M. Mecklenburg, X. N. Guan, A. Z. Stieg, B. C. Regan, D. C. Martin and R. B. Kaner, *J. Am. Chem. Soc.*, 2012, **134**, 9251–9262.
14 P. Li, Z. Qu, X. Chen, X. Huo, X. Zheng, D. Wang, W. Yang, L. Ji, P. Liu and X. Xu, *J. Mater. Chem. C*, 2017, **5**, 6216–6223.
15 H. Han, S. W. Lee, K. H. Moon and S. Cho, *ACS Omega*, 2019, **4**, 1244–1253.
16 J.-M. Yeh, K.-Y. Huang, S.-Y. Lin, Y.-Y. Wu, C.-C. Huang and S.-J. Liou, *J. Nanotechnol.*, 2009, **2009**, 217469.
17 X.-k. Kong, Z.-y. Sun, M. Chen, C.-l. Chen and Q.-w. Chen, *Energy Environ. Sci.*, 2013, **6**, 3260–3266.
18 X.-F. Zhang, X.-Y. Zhu, J.-J. Feng and A.-J. Wang, *Appl. Surf. Sci.*, 2018, **428**, 798–808.
19 Y. Li, J. Y. Lan, J. Liu, J. Yu, Z. Luo, W. Wang and L. Sun, *Ind. Eng. Chem. Res.*, 2015, **54**, 5656–5663.
20 G.-H. Lai, T.-C. Huang, Y.-H. Pai, B.-S. Huang, M.-H. Tsai, T.-I. Yang and Y.-H. Chung, *J. Taiwan Inst. Chem. Eng.*, 2019, **95**, 525–531.

21 Y.-Y. Ou and M. H. Huang, *J. Phys. Chem. B*, 2006, **110**, 2031–2036.
22 H. Yao, L. Jin, H.-J. Sue, Y. Sumi and R. Nishimura, *J. Mater. Chem. A*, 2013, **1**, 10783–10789.
23 H. Yao, T.-C. Huang and H.-J. Sue, *RSC Adv.*, 2014, **4**, 61823–61830.
24 G. H. Lai, T. C. Huang, I. H. Tseng, B. S. Huang, T. I. Yang and M. H. Tsai, *eXPRESS Polym. Lett.*, 2019, **13**, 772–784.
25 P. Li, T.-C. Huang, K. L. White, S. Hawkins, M. Kotaki, R. Nishimura and H.-J. Sue, *RSC Adv.*, 2015, **5**, 102633–102642.
26 B.-S. Huang, G.-H. Lai, T.-I. Yang, M.-H. Tsai and Y.-C. Chou, *Polymers*, 2020, **12**, 91.
27 H.-L. Guo, X.-F. Wang, Q.-Y. Qian, F.-B. Wang and X.-H. Xia, *ACS Nano*, 2009, **3**, 2653–2659.
28 Y.-H. Yu, Y.-Y. Lin, C.-H. Lin, C.-C. Chan and Y.-C. Huang, *Polym. Chem.*, 2014, **5**, 535–550.
29 L.-C. Yeh, T.-C. Huang, Y.-J. Lin, G.-H. Lai, T.-I. Yang, A.-Y. Lo and J.-M. Yeh, *Int. J. Green Energy*, 2016, **13**, 1334–1341.
30 H.-Y. Huang, J.-W. Jian, Y.-T. Lee, Y.-T. Li, T.-C. Huang, J.-H. Chang, L.-C. Yeh and J.-M. Yeh, *Polymer*, 2012, **53**, 4967–4976.
31 L.-C. Yeh, T.-C. Huang, F.-Y. Lai, G.-H. Lai, A.-Y. Lo, S.-C. Hsu, T.-I. Yang and J.-M. Yeh, *Surf. Coat. Technol.*, 2016, **303**, 154–161.
32 T.-C. Huang, L.-C. Yeh, G.-H. Lai, B.-S. Huang, T.-I. Yang, S.-C. Hsu, A.-Y. Lo and J.-M. Yeh, *Int. J. Green Energy*, 2017, **14**, 113–120.
33 Y. Ding, J. Liang, G. Liu, W. Ni and L. Shen, *Coatings*, 2019, **9**, 399.
34 S. Wang, D. Chao, E. B. Berda, X. Jia, R. Yang, X. Wang, T. Jiang and C. Wang, *RSC Adv.*, 2013, **3**, 4059–4065.
35 H.-Y. Huang, T.-C. Huang, J.-C. Lin, J.-H. Chang, Y.-T. Lee and J.-M. Yeh, *Mater. Chem. Phys.*, 2013, **137**, 772–780.
36 T. Liu, J. Li, X. Li, S. Qiu, Y. Ye, F. Yang and H. Zhao, *Prog. Org. Coat.*, 2019, **128**, 137–147.
37 A. A. Salem and B. N. Grgur, *Prog. Org. Coat.*, 2018, **119**, 138–144.
38 J. Zhu, H.-f. Du, Q. Zhang, J. Zhao, G.-j. Weng, J.-j. Li and J.-w. Zhao, *J. Mater. Chem. C*, 2019, **7**, 3322–3334.
39 J. Chen, B. Yao, C. Li and G. Shi, *Carbon*, 2013, **64**, 225–229.
40 T.-C. Huang, L.-C. Yeh, H.-Y. Huang, Z.-Y. Nian, Y.-C. Yeh, Y.-C. Chou, J.-M. Yeh and M.-H. Tsai, *Polym. Chem.*, 2014, **5**, 630–637.
41 T. C. Huang, L. C. Yeh, G. H. Lai, F. Y. Lai, T. I. Yang, Y. J. Huang, A. Y. Lo and J. M. Yeh, *eXPRESS Polym. Lett.*, 2016, **10**, 450–461.
42 L. Qin, H. Yi, G. Zeng, C. Lai, D. Huang, P. Xu, Y. Fu, J. He, B. Li, C. Zhang, M. Cheng, H. Wang and X. Liu, *J. Hazard. Mater.*, 2019, **380**, 120864.
43 M.-H. Tsai, I. H. Tseng, J.-C. Chiang and J.-J. Li, *ACS Appl. Mater. Interfaces*, 2014, **6**, 8639–8645.
44 P. Kar, S. Sardar, B. Liu, M. Sreemany, P. Lemmens, S. Ghosh and S. K. Pal, *Sci. Technol. Adv. Mater.*, 2016, **17**, 375–386.
45 L.-C. Yeh, T.-C. Huang, Y.-P. Huang, H.-Y. Huang, H.-H. Chen, T.-I. Yang and J.-M. Yeh, *Electrochim. Acta*, 2013, **94**, 300–306.
46 H.-Y. Huang, Y.-T. Lee, L.-C. Yeh, J.-W. Jian, T.-C. Huang, H.-T. Liang, J.-M. Yeh and Y.-C. Chou, *Polym. Chem.*, 2013, **4**, 343–350.
47 M. H. Tsai, S. H. Lu, Y. H. Lai, G. H. Lai, G. V. Dizon, T. I. Yang, Y. J. Lin and Y. C. Chou, *eXPRESS Polym. Lett.*, 2018, **12**, 71–81.
48 P. Deng, Z. Xu, Y. Feng and J. Li, *Sens. Actuators, B*, 2012, **168**, 381–389.
49 A. Verma, S. Kumar, W.-K. Chang and Y.-P. Fu, *Dalton Trans.*, 2020, **49**, 625–637.
50 H. G. Soğukömeroğulları, Y. Karataş, M. Celebi, M. Gülcan, M. Sönmez and M. Zahmakiran, *J. Hazard. Mater.*, 2019, **369**, 96–107.
51 T. Wi-Afedzi, F.-Y. Yeoh, M.-T. Yang, A. C. K. Yip and K.-Y. A. Lin, *Sep. Purif. Technol.*, 2019, **218**, 138–145.
52 H. Koga and T. Kitaoka, *Chem. Eng. J.*, 2011, **168**, 420–425.
53 D. Xu, P. Diao, T. Jin, Q. Wu, X. Liu, X. Guo, H. Gong, F. Li, M. Xiang and Y. Ronghai, *ACS Appl. Mater. Interfaces*, 2015, **7**, 16738–16749.
54 Z.-S. Lv, X.-Y. Zhu, H.-B. Meng, J.-J. Feng and A.-J. Wang, *J. Colloid Interface Sci.*, 2019, **538**, 349–356.
55 Y. Ma, X. Wu and G. Zhang, *Appl. Catal., B*, 2017, **205**, 262–270.
56 L. Qin, Z. Zeng, G. Zeng, C. Lai, A. Duan, R. Xiao, D. Huang, Y. Fu, H. Yi, B. Li, X. Liu, S. Liu, M. Zhang and D. Jiang, *Appl. Catal., B*, 2019, **259**, 118035.
57 Y. Xu, F. Zhou, M. Chen, H. Hu, L. Lin, J. Wu and M. Zhang, *New J. Chem.*, 2020, **44**, 9793–9801.
58 W.-J. Liu, K. Tian, H. Jiang and H.-Q. Yu, *Green Chem.*, 2014, **16**, 4198–4205.
59 X.-Y. Zhu, Z.-S. Lv, J.-J. Feng, P.-X. Yuan, L. Zhang, J.-R. Chen and A.-J. Wang, *J. Colloid Interface Sci.*, 2018, **516**, 355–363.
60 M. Liu, H. Yang, Z. Xu, W. Ma, F. Cui, G. Lu, L. Xu and T. Cui, *New J. Chem.*, 2020, **44**, 7035–7041.
61 S. R. Thawarkar, B. Thombare, B. S. Munde and N. D. Khupse, *RSC Adv.*, 2018, **8**, 38384–38390.
62 H. Liu and Q. Yang, *J. Mater. Chem.*, 2011, **21**, 11961–11967.
63 E. Abroushan, S. Farhadi and A. Zabardasti, *RSC Adv.*, 2017, **7**, 18293–18304.
64 Y. Zhou, H. Ding, J. Liu, A. M. LaChance, M. Xiao, Y. Meng and L. Sun, *Adv. Compos. Hybrid Mater.*, 2019, **2**, 520–529.
65 G.-H. Lai, B.-S. Huang, T.-I. Yang, M.-H. Tsai and Y.-C. Chou, *Polymer*, 2020, 123200, DOI: 10.1016/j.polymer.2020.123200.